PCCP

Accepted Manuscript

This is an *Accepted Manuscript*, which has been through the Royal Society of Chemistry peer review process and has been accepted for publication.

Accepted Manuscripts are published online shortly after acceptance, before technical editing, formatting and proof reading. Using this free service, authors can make their results available to the community, in citable form, before we publish the edited article. We will replace this *Accepted Manuscript* with the edited and formatted *Advance Article* as soon as it is available.

You can find more information about *Accepted Manuscripts* in the Information for Authors.

Please note that technical editing may introduce minor changes to the text and/or graphics, which may alter content. The journal's standard Terms & Conditions and the Ethical guidelines still apply. In no event shall the Royal Society of Chemistry be held responsible for any errors or omissions in this *Accepted Manuscript* or any consequences arising from the use of any information it contains.

ROYAL SOCIETY OF CHEMISTRY

www.rsc.org/pccp

Tailoring the electronic structure of β-Ga_2O_3 by non-metal doping from hybrid density functional theory calculations

Weiyan Guo [a], Yating Guo [a], Hao Dong [a,*] , Xin Zhou [b,*]

[a] Institute of Chemistry for Functionalized Materials, School of Chemistry and Chemical Engineering, Liaoning Normal University, Dalian, Liaoning 116029, China

[b] State Key Laboratory of Catalysis, Dalian Institute of Chemical Physics, Chinese Academy of Sciences, Dalian National Laboratory for Clean Energy, Dalian, Liaoning 116023, China

* Corresponding author.

E-mail addresses: sinodonghao@gmail.com (H. Dong) xzhou@dicp.ac.cn (X. Zhou)

Physical Chemistry Chemical Physics Accepted Manuscript

Abstract

A systematic study using density functional theory has been performed for β-Ga_2O_3 doped with non-metal elements X (X=C, N, F, Si, P, S, Cl, Se, Br, and I) to evaluate the effect of doping on the band edges and photocatalytic activity of β-Ga_2O_3. The utilization of a more reliable hybrid density functional as prescribed by Heyd, Scuseria and Ernzerhof, is found to be effective in predicting the band gap of β-Ga_2O_3 (4.5 eV) in agreement with the experimental result (4.59 eV). Based on the relaxed structures of X-doped systems, the defect formation energies and the plots of density of states have been calculated to analyze the band edges, the band gap states and the preferred doping sites. Our results show that the doping is energetically favored under Ga-rich growth condition with respect to O-rich growth condition. It is easier to replace the threefold coordinated O atom with non-metal elements than the fourfold coordinated O atom. X-doped systems (X=C, Si, P) show no change of band gap, with the presence of discrete midgap states, which have adverse effect on the photocatalytic property. The photocatalytic redox ability can be improved to a certain extent by doping with N, S, Cl, Se, Br, and I. The band alignments for Se-doped and I-doped β-Ga_2O_3 are well positioned for the feasibility of both photo-oxidation and photo-reduction of water, which are promising photocatalysts for water splitting in the visible region.

Physical Chemistry Chemical Physics Accepted Manuscript

1. Introduction

Photocatalytic overall water splitting is one of the most attractive approaches to solving energy and environmental issues at a global level, and drawing increasing worldwide attention. Over the past several decades, a large number of semiconductor-based photocatalysts have been developed and reported to exhibit photocatalytic activities for splitting water.[1-8] However, most of these materials are only active in ultraviolet region, which merely occupied about 5% of the solar spectrum. In order to improve the solar energy utilization, numerous investigations have attempted to extend the absorption wavelength range of photocatalysts.[9-16] Among them, doping of a foreign element into active photocatalysts with wide band gaps is the well-studied way to design the visible-light-driven photocatalyst.[13-16] During the doping process, dopants may be introduced into the lattice of semiconductors, or react with the parent semiconductor to form a new surface nanostructure.[2,13,17,18] It was found that doping is not always effective in enhancing the photocatalytic activity.[19-22] A deep understanding of the effects of doping foreign ion on the structure, charge carrier kinetics and activity of the photocatalysts is definitely necessary. The description of these effects is very delicate from the theoretical point of view, especially concerning the possible configurations after doping and the details of electronic structures. [23-28]

Among the developed photocatalysts, semiconductors with a d^{10} electron configuration exhibit superior photocatalytic activities,[29-32] mainly because their conduction bands are formed by hybridized sp orbitals with large dispersion able to generate photoexcited electrons with large mobility.[4] Gallium oxide (Ga_2O_3) is a

Physical Chemistry Chemical Physics Accepted Manuscript

representative of such d^{10} metal oxides, exhibiting high activity of overall water splitting and degradation of organic pollutants. [33-37] Ga_2O_3 can adopt five different crystalline structures controlled by preparative means, designated as α, β, γ, δ, and ε phases.[38] The relative order of stability of different phases has been predicted by density functional theory (DFT) calculations, which is in good agreement with experimental results.[39-42] In these phases, β-Ga_2O_3 has drawn much attention as the most stable crystal phase.[33-36,43] β-Ga_2O_3 is a wide band gap semiconductor, with the conduction band minimum (CBM) lower than the H^+/H_2 potential (0 eV) and the valence band maximum (VBM) higher than the O_2/H_2O potential (1.23 eV). The appropriate band position of β-Ga_2O_3 provides one of the requirements for an energetically-feasible overall water splitting reaction. Doping with non-metal anions has been considered for more than ten years as a promising way to change the photo-absorption properties of photocatalysts by influencing the electronic structure of semiconductors.[44-49] It was found that, in Sn-doped and Si-doped β-Ga_2O_3 grown by different experimental methods, Sn and Si behave as n-type donor.[50-52] Liu *et al.* prepared N-doped β-Ga_2O_3 nanowires by CVD, which has a p-type electrical conductivity.[53] Also nitrogen element doping can enable tunable light emission.[54,55] Theoretical calculations were performed to calculate the electronic, magnetic and optical properties of nitrogen-doped β-Ga_2O_3, showing that the N 2p states contribute the experimental red-shift of absorption band edge.[56,57] However, there is no report about the photocatalytic performance of non-metal doped β-Ga_2O_3 experimentally.

In this work, we present a systematic comparative study of the non-metal doping of

Physical Chemistry Chemical Physics Accepted Manuscript

bulk β-Ga_2O_3 by some elements in the second to fifth row of the periodic table (C, N, F, Si, P, S, Cl, Se, Br and I). Only substitutional doping of O atom in the lattice has been considered. The main aim of this study is to identify and rationalize the trends along the series, to discuss the stability of the different doping cases based on the calculated formation energies, and to explore how the CBM and VBM of pure β-Ga_2O_3 are influenced by the dopants and whether the doping introduces band gap states.

2. Computational Details

All the spin-polarized DFT calculations were performed with the VASP (Vienna Ab initio Simulation Package) code.[58,59] The exchange correlation potential was described by the Perdew-Burke-Ernzerhof (PBE) functional within the generalized gradient approximation (GGA).[60] The projector-augmented wave method was applied to describe electron-ion interactions.[61,62] Full optimization of the cell parameters for the bulk *β*-Ga_2O_3 with monoclinic structure was carried out by using the 3×11×7 Monkhorst-Pack type *k*-point sampling. The cutoff energy for the plane wave basis set was fixed at 520 eV. The calculated lattice parameters, *a*=12.504 Å, *b*=3.101 Å, *c*=5.915 Å, and β=103.71°, are in good agreement with experimental data.[63] A 1×2×1 supercell with 40 atoms was used to simulate the bulk *β*-Ga_2O_3. A Monkhorst-Pack set of 3×7×7 *k*-points was applied. The geometries were considered to be converged when the forces on each ion become 0.01 eV/ Å or less.

Based on relaxed geometries by the GGA-PBE method, a more accurate screened Coulomb hybrid functional HSE06 presented by Heyd, Scuseria and Ernzerhof is

Physical Chemistry Chemical Physics Accepted Manuscript

adopted to finish the electronic structure calculations.[64-66] The HSE06 functional includes a fraction α, of screened, short-range HF exchange to improve the derivative discontinuity of the Kohn-Sham potential for integer electron numbers. The percentage of HF exchange in a hybrid functional is not a universal constant and the optimal value may be system-dependent. The band gap of bulk β-Ga_2O_3 from experiment is 4.2-4.7 eV.[34,36,67,68] In this work, α is set to 0.3 because we found that this value can yield close agreement between the computed (4.5 eV) and experimental band gaps.

3. Results and Discussion

3.1. Bulk β-Ga_2O_3

Figure 1a shows that the supercell of β-Ga_2O_3 contains eight Ga_2O_3 formula units with two nonequivalent Ga sites and three nonequivalent O sites. Ga1 is bonded to four O anions in the form of a distorted tetrahedron, and Ga2 forms highly distorted octahedral with six O anions. Each O1 is threefold coordinated and lies at the intersection of two tetrahdra and one octahedron. Each O2 is fourfold coordinated and connected with three octahedral and one tetrahedron. Each O3 is threefold coordinated and shared between two octahedra and one tetrahedron. The calculated bond lengths are as follows: Ga1-O1=1.867 Å, Ga1-O2=1.894 Å, Ga1-O3= 1.864 Å, Ga2-O1=1.951 Å, Ga2-O2=2.073 Å, Ga2-O3= 1.969 Å, which are in good agreement with experimental values.[63]

To modify the band structure of Ga_2O_3 through doping, we first need to know the atomic wave function characters of the band-edge states. As can be seen from the

Physical Chemistry Chemical Physics Accepted Manuscript

calculated total density of states (TDOS) and partial density of states (PDOS) for bulk β-Ga_2O_3 in Figure 1(b), the VBM is mainly composed of O 2p states, slightly hybridized with Ga 3d and Ga 4p states; while the CBM consists mostly of Ga 4s states. The strong mixing of O and Ga orbitals is indicative of the high degree of covalent bonding in this semiconductor. The band gap of is computed to be 4.5 eV by means of the HSE method, which is close to the experimental results.[36,67,68]

3.2. Formation energies

We have considered three different configurations for each doped system by introducing non-metal atom at the O1, O2 and O3 positions, respectively (Figure 1a). To get an idea about the stability of the doped systems, we calculated the formation energy (E_f) according to the following equation

$$E_f = E_{X-doped} + \mu_O - E_{undoped} - \mu_X \qquad (1)$$

where $E_{X-doped}$ and $E_{undoped}$ are total energies of the supercells with and without dopants, respectively. The quantities μ_O and μ_X represent the chemical potential for oxygen and X atoms, respectively. The chemical potential of O depends on the nature of synthesis condition of Ga_2O_3. In the case of Ga_2O_3, the chemical potential of the constituent elements must satisfy the relationship

$$2\mu_{Ga} + 3\mu_O = \mu_{Ga2O3} \qquad (2)$$

Under the environment of O-rich condition, μ_O is calculated from the energy of O atom. In the case of Ga-rich condition, μ_{Ga} is obtained from the energy of the Ga atom in the bulk crystal and μ_O is determined from Eq. (2). The chemical potential μ_X is obtained from the energy calculated for one X atom in a cubic unit cell with side

Physical Chemistry Chemical Physics Accepted Manuscript

length of 15Å. The calculated formation energies in X-doped systems are summarized in Table 1.

It is noted from Eq (1) that the substitutional doping is energetically more favorable as the E_f value becomes smaller. From the E_f value of Table 1, the following trends are observed:

(a) The doping is energetically favored under Ga-rich growth conditions with respect to the O-rich growth conditions.

(b) Comparing the relative energies of three configurations for each doped system, it is found that O2 site is energetically unfavorable for all the cases. In other words, it is difficult to replace the fourfold coordinated O atom with other non-metal atoms.

(c) As to the substitutional nonmetal X (X= C, N and Si), doping at O1 site is calculated to be energetically most favorable. For nonmetal species X (X=F, Cl, Br, I, P, S and Se), O3 site is found to be the most stable site for doping.

(d) The doping becomes more difficult as the size of atom increases in the same group, such as C < Si, F < Cl < Br < I.

In order to prove the rationality of our current model, we chose a larger supercell including 80 atoms to calculate the formation energy for each impurity case. The results are shown in parentheses in Table 1. As can be seen, compared with the small supercell, a larger supercell produces the same trend on the most stable doping site for every system. Therefore, we will use the current model including 40 atoms to discuss the geometrical and electronic structures.

Physical Chemistry Chemical Physics Accepted Manuscript

3.3. Geometrical Structures and Electronic Structures

The optimized geometries of local structure for every doping case are shown in Figure 2. The calculated TDOS and PDOS for doped systems are displayed in Figure 3, 4 and 5, where the zero energy value is set at the top of the valence band in order to easily allow identification of the band gap and of the relative position of the impurity states introduced by dopants.

3.3.1. Doping by Group IV-A Elements

For C-doped Ga_2O_3, the optimized Ga-C bonds of the local "Y-shaped" CGa_3 structure are longer than the corresponding Ga-O bonds of undoped Ga_2O_3 (1.983 vs 1.951 Å, and 1.943 vs 1.867 Å). The larger expansion of the local structure reflects the fact that the C atom has a larger atomic radius than does the O atom (0.7 vs 0.6 Å). [69] As shown in Figure 2(a), the distortion mainly results from the fact that C atom and the adjacent O atom at O1 site approach each other, which makes the distance between C and O atoms to be 1.570 Å. The C 2p orbitals are higher in energy than O 2p orbitals because their nuclear charges are smaller. When a C atom replaces an O atom in the Ga_2O_3 structure, isolated C 2p states appear into the band gap (see Figure 3). The Fermi energy of the system corresponds to the highest C 2p state, which is 1.58 eV above the VBM. There is almost no change of the band gap for C doping with respect to pure Ga_2O_3. Due to the symmetric contribution of spin up and spin down for C 2p states, the overall spin configuration of the system becomes a closed shell singlet.

In the case of Si-doped Ga_2O_3, the Ga-Si bond lengths of the local "Y-shaped"

Physical Chemistry Chemical Physics Accepted Manuscript

$SiGa_3$ structure are 2.222 and 2.223 Å, much larger than Ga-O bonds in pure Ga_2O_3 (1.951 and 1.867 Å) due to the relative larger atomic radius of Si than that of O, indicating that the Si doping induces relative larger local structure modifications. Similar to the local structure of C-doped Ga_2O_3, the movement of Si to the neighboring O atoms decreases the distance to 1.815 Å. As shown in Figure 3, substitution of Si at the O1 site brings no change of VBM and CBM compared to the undoped case. The Fermi energy is set at 2.2 eV above the VBM and the isolated Si 3d states in the middle of the band gap is entirely below the Fermi level. The symmetric spin-up and spin-down contributions make the system a closed shell singlet.

3.3.2. Doping by Group V-A Elements

The most stable configuration for N-doped Ga_2O_3 is doping at the O1 site. Replacing an O with an N atom does not result in significant structural changes as shown Figure 2(c). The Ga-N bond lengths, 1.963 and 1.901 Å, are only slightly longer than the Ga-O ones, 1.951 and 1.867 Å. As can be seen from Figure 3, the N 2p orbitals split into occupied and unoccupied states, mixing well with O 2p orbitals at the VBM and located at the "forbidden gap" near to the CBM. These states accommodate five valence electrons of N dopant. As a result, the unoccupied N 2p state is responsible for the band gap narrowing of 0.7 eV with respect to that of pure Ga_2O_3.

For P-doped Ga_2O_3, the calculated formation energies in Table 1 indicate that replacing O3 atom with P atom is energetically more favorable. The computed Ga-P

Physical Chemistry Chemical Physics Accepted Manuscript

bond lengths are 2.337 and 2.212 Å, respectively, which are much longer than the original Ga-O bonds (1.969 and 1.864 Å). There are two possible reasons responsible for this change. One arises from the larger atomic radius of the P relative to the O ion, and the other is the lower electronegativity of the P atom in comparison to the O atom, which leads to a decrease in electron cloud overlapping and weakens the strength of the Ga-P bond, as well as elongating the Ga-P bond length. For subsitutional P to O doping, Figure 3 shows little shift of the position of the VBM and CBM with respect to the undoped material. The most of P 3p states lie in the band gap and form occupied and unoccupied energy bands.

3.3.3. Doping by Higher Chalcogens

Since Ga_2O_3 is an oxide, oxygen-doping is not practical, but there is interest in doping with sulfur and selenium. Because of the relatively larger atomic radius of S and Se compared to O (1.0 vs 0.6 Å, 1.15 vs 0.6 Å), this is expected to induce a large atomic reorganization. The S and Se atoms move slightly out of the hexagon shown in Figure 2(e) and 2(f) so that the Ga-S bond lengths (2.284 and 2.182 Å) and the Ga-Se bond lengths (2.362 and 2.267 Å) are larger than the Ga-O ones (1.969 and 1.864 Å). As shown in Figure 4, since the total number of electrons remain the same after replacing O with S or Se atom, the overall VBM and CBM profiles look symmetric and clean for both S-doping and Se-doping cases. The VBM edge of S-doped system is shifted upwards by 0.98 eV and mainly composed of the S 3p orbitals, whereas the CBM remains almost unchanged. Thus, the effective band gap of S-doped system is 3.52 eV. For Se-doped Ga_2O_3, the highest occupied level moves upwards significantly,

Physical Chemistry Chemical Physics Accepted Manuscript

by 1.68 eV, due to the much higher energy of Se 4p compared to the O 2p orbitals. While the CBM keeps almost at its original position. Consequently, the calculated band gap of Se-doped Ga_2O_3 is 2.80 eV.

3.3.4. Halogen Doping

The effect of an X-dopant (X=F, Cl, Br and I) on the structure of X-doped Ga_2O_3 can be seen from the local geometry around X, as displayed in Figure 2. The calculated Ga1-X and Ga2-X bond lengths are 1.964 and 2.144 Å for F, 2.456 and 2.371 Å for Cl, 2.689 and 2.434 Å for Br, and 2.800 and 2.542Å for I, respectively, which are longer than those in the undoped Ga_2O_3. In the F-doped and undoped cases, Ga1-X bonds are shorter than Ga2-X bonds. While in the X-doped systems (X=Cl, Br, and I), Ga1-X bonds become longer than Ga2-X bonds. The reason for this change is that the "Y-shaped" XGa3 has a local C_s symmetry with the Ga1-X bond in the mirror plane of symmetry and two Ga2-X bonds out of plane and symmetric to each other. As X atom becomes larger, the Ga1-X length increases faster than does the Ga2-X length.

Several experimental investigations showed that there is no change in the optical adsorption edge of oxides upon F-doping since the F 2p orbitals are lower in energy than the O 2p orbitals.[70-72] Our results in Figure 5 suggest that for Ga_2O_3, doping F also does not change the initial positions of VBM and CBM. For Cl-doped Ga_2O_3, the VBM is raised by 0.13 eV, while the CBM is lowered by about 0.35 eV. The PDOS in Figure 5 shows that Cl 3p orbitals contribute importantly to the reduction of the band gap. For subtitutional Br to O, the Br 4p states locate just above the VBM and well

Physical Chemistry Chemical Physics Accepted Manuscript

overlap and mix with O 2p states. As a result, new edge of valence band shifts towards the higher energy by 0.52 eV. Meanwhile, the position of CBM is also effected and moves to the lower energy. Then, the effective band gap of Br-doped Ga_2O_3 is 3.44 eV. As can be seen from Figure 5, the VBM of I-doped system is raised strongly from that of pure Ga_2O_3 by 1.65 eV due to the contribution of I 5p states, and the CBM shifts down by 0.21 eV, which results in the band gap narrowing of 1.86 eV.

3.3.5. Charge Distribution Analysis

To provide insight regarding the nature of chemical bonding between the doping atom and Ga_2O_3 bulk, charge density differences for the most stable doping configuration of each case have been calculated as

$$\Delta\rho = \rho(\text{X-doped}) - \rho(Ga_2O_3) - \rho(\text{X}) \qquad (3)$$

Where ρ(X-doped) is the total charge density of the X-doped Ga_2O_3 system, $\rho(Ga_2O_3)$ is the charge density of the Ga_2O_3 bulk after doping except X atom, and ρ(X) is the electron density of the X atom isolated in the same periodic box. As shown in Figure 6, for C-doped and Si-doped systems, the electron density accumulates along the C-O and Si-O bonds, which corresponds to a new C/Si-O bond formed. In N-doped Ga_2O_3, the electron density is depleted along the Ga-N bonds, which leads to the increase of Ga-N bonds on the basis of the Ga-O bonds in Ga_2O_3 bulk. For P-doped, S-doped, Se-doped, Cl-doped, Br-doped and I-doped, the charge density difference maps look very similar and reveal that strong depletion of electron density between the impurity atom and bonded Ga atoms pointing to strong antibonding character, which is in good agreement with the longer Ga-X bonds compared with the Ga-O in the pure Ga_2O_3.

Physical Chemistry Chemical Physics Accepted Manuscript

As to F-doped case, the electron density displayed in Figure 6(g) is localized along the Ga-F bonds, and bonding interaction between Ga and F atoms results in relatively small deformation of the localized structure compared with other doping systems.

3.4. Prediction on Photocatalytic Applications

In the photocatalytic overall water-splitting reactions, the photo-genenerated electrons and holes cause redox reactions similarly to electrolysis. Water molecules are reduced by the electrons to form H_2 and are oxidized by the holes to from O_2. Important points in the semiconductor photocatalyst materials are the width of the band gap and levels of the conduction and valence bands. To make efficient use of the visible light, the semiconductor band gap should be smaller than 3.0 eV. The CBM has to be more negative than the reduction potential of H^+/H_2 (0 V vs. NHE), whereas the VBM has to be more positive than the oxidation potential of O_2/H_2O (1.23 V).

In order to evaluate the physical significance of this work, the calculated results and analysis are presented in the form of schematic diagram in Figure 7. According to experimental measurements,[73] the rough conduction band edge potential of pure β-Ga_2O_3 is -1.55 V with respect to NHE. Subsequently the valance band edge position is determined as 2.95 V based on the calculated band gap of 4.5 eV. To assess the photocatalytic performance, we have aligned the CBM and VBM energy levels of X-doped systems obtained from the corresponding TDOS plots by taking into account the relative location with respect to the undoped Ga_2O_3. As shown in Figure 7, for C, Si and P-doped systems, some impurity states are localized in the middle of band gap, which are detrimental for photocatalysis because the gap states can act as

Physical Chemistry Chemical Physics Accepted Manuscript

recombination centers to limit the efficiency of semiconductors. Replacing O with F exerts no effect on the band-gap narrowing. For N-doped Ga_2O_3, the photo-reduction ability is supposed to be improved since the CBM shifts downwards by 0.7 eV with respect to pure Ga_2O_3. Doping with isovalent elements (S and Se) essentially influences the position of VBM and greatly enhanced the photo-oxidation capacity. For Se-doped system, the absorption edge moves from UV to visible light range. As to halogen doping, including Cl, Br and I, both photo-reduction and photo-oxidation abilities are improved since the positions of CBM and VBM move towards the energy levels of water reduction and oxidation simultaneously. Our calculations indicate that I-doped Ga_2O_3 can be photocatalytically active under visible light.

Further experiments should therefore be done for Se-doped and I-doped Ga_2O_3 to systemically investigate their photocatalytic properties. Certainly, the photocatalytic activities of Ga_2O_3 don't only depend on its bulk properties, in particular, the nature of its surface is also an important factor, however it is beyond the scope of present work. We will further investigate the relationship between the photocatalytic activities and surface properties as well as the effect of loading cocatalysts in future work.

4. Conclusions

In the present first-principles DFT study on the energetic and electronic structures of X-doped β-Ga_2O_3 (X=C, N, F, Si, P, S, Cl, Se, Br, and I), we considered the substitutional doping at oxygen sites. Our results lead to the following conclusions:

(1) The doping energetically more favorable under Ga-rich growth conditions than under O-rich growth conditions.

Physical Chemistry Chemical Physics Accepted Manuscript

(2) The comparison of formation energies doping at different oxygen sites suggests that it is the most difficult to replace the fourfold coordinated O atom with non-metal atoms.

(3) For X-doped Ga_2O_3 (X=N, S, Se, Cl, Br, I), clean and narrowed band gaps are obtained. Meanwhile, photocatalytic reduction or/and oxidation abilities are improved with respect to pure Ga_2O_3.

(4) Se-doped and I-doped β-Ga_2O_3 are promising candidates for visible-light photocatalysts owing to the largest band gap narrowing and increase of photocatalytic redox ability.

Acknowledgements

Dr. Dong gratefully acknowledges the financial support from the National Science Foundation of China under Grant 21303079. Dr. Zhou appreciates the funding support by the National Science Foundation of China under Grant 21473183.

References

1 A. Fujishima and K. Honda, *Nature*, 1972, **238**, 37-38.

2 H. Kato, K. Asakura and A. Kudo, *J. Am. Chem. Soc.*, 2003, **125**, 3082-2089.

3 K. Maeda, T. Takata, M. Hara, N. Saito, Y. Inoue, H. Kobayashi and K. Domen, *J. Am. Chem. Soc*., 2005, **127**, 8286-8287.

4 Y. Inoue, *Energy Environ. Sci*., 2009, **2**, 364-386.

5 A. Kudo and Y. Miseki, *Chem. Soc. Rev.*, 2009, **38**, 253-278.

6 Y. Inoue, *Energy Environ. Sci*., 2009, **2**, 364-386.

7 K. Maeda, M. Higashi, D. Lu, R. Abe and K. Domen, *J. Am. Chem. Soc*., 2010, **132**, 5858-5868.

8 X. Chen, S. Shen, L. Guo and S. S. Mao, *Chem. Rev*., 2010, **110**, 6503-6570.

9 X. Wang, K. Maeda, A. Thomas, K. Takanabe, G. Xin, J. M. Carlsson, K. Domen

Physical Chemistry Chemical Physics Accepted Manuscript

and M. Antonietti, *Nat. Mater.*, 2009, **8**, 76-80.

10 R. Abe, *J. Photochem. Photobiol. C: Photochem. Rev.*, 2010, **11**, 179-209.

11 K. Iwashina and A. Kudo, *J. Am. Chem. Soc*., 2011, **133**, 13272-13275.

12 S. X. Ouyang, H. Tong, N. Umezawa, J. Cao, P. Li, Y. P. Bi, Y. J. Zhang and J. H. Ye, *J. Am. Chem. Soc*., 2012, **134**, 1974-1977.

13 K. Maeda, H. Terashima, K. Kase, M. Higashi, M. Tabata and K. Domen, *Bull. Chem. Soc. Jpn*., 2008, **81**, 927-937.

14 Y. J. Zhang, A. Thomas, M. Antonietti and X. C. Wang, *J. Am. Chem. Soc.*, 2009, **131**, 50-51.

15 X. B. Chen, L. Liu, Y. Y. Peter and S. S. Mao, *Science*, 2011, **331**, 746-750.

16 W. J. Jo, J. W. Jang, K. J. Kong, H. J. Kang, J. Y. Kim, H. Jun, K. P. S. Parmar and J. S. Lee, *Angew. Chem., Int. Ed*., 2012, **51**, 3147-3151.

17 A. Iwase, H. Kato, H. Okutomi and A. Kudo, *Chem. Lett*., 2004, 1260-1261.

18 T. Takata and K. Domen, *J. Phys. Chem. C*, 2009, **113**, 19386-19388.

19 H. Irie, Y. Maruyama and K. Hashimoto, *J. Phys. Chem. C*, 2007, **111**, 1847-1852.

20 Y. Sakata, Y. Matsuda, T. Yanagida, K. Hirata, H. Imamura and K. Teramura, *Catal. Lett*. 2008, **125**, 22-26.

21 R. Ullah, H. Q. Sun, H. M. Ang, M. O. Tade and S. B. Wang, *Catal. Today*, 2012, **192**, 203-212.

22 K. Shimura and H. Yoshida, *Phys. Chem., Chem. Phys*., 2012, **14**, 2678-2684.

23 C. Di Valentin, G. Pacchioni and A. Selloni, *J. Phys. Chem. C*, 2009, **113**, 20543-20552.

24 R. Long and N. J. English, *Chem. Mater*., 2010, **22**, 1616-1623.

25 W.-J. Yin, S.-H. Wei, M. M. Al-Jassim and Y. Yan, *Phys. Rev. Lett*., 2011, **106**, 066801.

26 Z. D. Pozun and G. Henkelman, *J. Chem. Phys*., 2011, **134**, 224706.

27 P. Liu, J. Nisar, B. Pathak and R. Ahuja, *Int. J. Hydrogen Energy*, 2012, **37**, 11611- 11617.

28 J. Wang, H. Sun, J. Huang, Q. Li and J. Yang, *J. Phys. Chem. C*, 2014, **118**, 7451-7457.

Physical Chemistry Chemical Physics Accepted Manuscript

29 J. Sato, H. Kobayashi, N. Saito, H. Nishiyama and Y. Inoue, *J. Photochem. Photobiol. A*, 2003, **158**, 139 -144.

30 J. Sato, N. Saito, H. Nishiyama and Y. Inoue, *J. Phys. Chem. B*, 2001, **105**, 6061-6063.

31 J. Sato, N. Saito, H. Nishiyama and Y. Inoue, *J. Photochem. Photobiol. A*, 2002, **148**, 85-89.

32 K. Ikarashi, J. Sato, H. Kobayashi, N. Saito, H. Nishiyama, Y. Simodaira and Y. Inoue, *J. Phys. Chem. B*, 2005, **109**, 22995-23000.

33 T. Yanagida, Y. Sakata and H. Imamura, *Chem. Lett*., 2004, **33**, 726-727.

34 X. Wang, Q. Xu, M. Li, S. Shen, X. Wang, Y. Wang, Z. Feng, J. Shi, H. Han and C. Li, *Angew. Chem., Int. Ed.*, 2012, **51**, 13089-13092.

35 Y. Hou, J. Zhang, Z. Ding and L. Wu, *Powder Technol*. 2010, **203**, 440-446.

36 Y. Hou, L. Wu, X. Wang, Z. Ding, Z. Li and X. Fu, *J. Catal*. 2007, **250**, 12-18.

37 M. Muruganandham, R. Amutha, M. S. M. Abdel Wahed, B. Ahmmad, Y. Kuroda, R. P. S. Suri, J. J. Wu and M. E. T. Sillanpää, *J. Phys. Chem. C*, 2012, **116**, 44-53.

38 R. Roy, V. G. Hill and E. F. Osborn, *J. Am. Chem. Soc.*, 1952, **74**, 719-722.

39 H. He, R. Orlando, M. A. Blanco, R. Pandey, *Phys. Rev. B*, 2006, **74**, 195123-1-195123-8.

40 F. Litimein, D. Rached, R. Khenata, H. Baltache, *J. Alloys Comp.*, 2009, **488**, 148-156.

41 S. Yoshioka, H. Hayashi, A. Kuwabara, F. Oba, K. Matsunaga, I. Tanaka, *J. Phys.: Condens. Matter*, 2007, **19**, 346211-1-346211-11.

42 S. Md. Pratik, A. Nijamudheen, S. Bhattacharya, A. Datta, *Chem. Eur. J.*, 2014, 20, 3218-3224.

43 X. Wang, S. Shen, S. Jin, J. Yang, M. Li, X. Wang, H. Han and C. Li, *Phys. Chem., Chem. Phys*., 2013, **15**, 19380-19386.

44 B. Asahi, T. Morikawa, T. Ohwaki, K. Aoki and Y. Taga, *Science*, 2001, **293**, 269.

45 C. Di Valentin and G. Pacchioni, *Catal. Today*, 2013, **206**, 12-18.

46 M. V. Dozzi and E. Selli, *J. Photochem. Photobiol. C: Photochem. Rev*., 2013, **14**,

Physical Chemistry Chemical Physics Accepted Manuscript

13-28.

47 R. Marschall and L. Wang, *Catal. Today*, 2014, **225**, 111-135.

48 R. Long, Y. Dai, B. Huang, *Comput. Mater. Sci.*, 2009, **45**, 223-228.

49 R. Long, N. J. English, *Phys. Rev. B*, 2011, **83**, 155209-1-155209-5.

50 O. Masahiro and H. Hidenori, *Thin Solid Films*, 2002, **411**, 134-139.

51 O. Shigeo and S. Norihito, *Thin Solid Films*, 2008, **516**, 5763-5767.

52 J. G. Zhang and C. T. Xu, *J. Phys.-Chem.*, 2006, **67**, 1656-1659.

53 L. L. Liu, M. K. Li, D. Q. Yu, J. Zhang, H. Zhang, C. Qian and Z. Yang, *Appl. Phys. A*, 2010, **98**, 831-835.

54 J. L. F. Da Silva, A. Walsh and S.-H. Wei, *Phys. Rev. Lett.*, 2008, **100**, 256401-256406.

55 E. M. Julia, N. T. Emily and D. H. Michael, *Phys. Rev. B*, 2007, **76**, 155107-155114.

56 W.-Z. Xiao, L.-L. Wang, L. Xu, Q. Wan and A.-L. Pan, *Solid State Commun.*, 2010, **150**, 852-856.

57 L. Y. Zhang, J. L. Yan, Y. J. Zhang and T. Li, X. W. Ding, *Sci. China-Phys. Mech. Astron.*, 2012, **55**, 19-24.

58 G. Kresse and J.Furthmüller, *Phys. Rev. B*, 1996, **54**, 11169-11186.

59 G. Kresse and J.Furthmüller, *Comput. Mater. Sci.*, 1996, **6**, 15-50.

60 J. P. Perdew, K. Burke and M.Ernzerhof, *Phys. Rev. Lett.*, 1996, **77**, 3865-3868.

61 P. E. Blochl, *Phys. Rev. B*, 1994, **50**, 17953-17979.

62 G. Kresse and J. Joubert, *Phys. Rev. B*, 1999, **59**, 1758-1775.

63 S. Geller, *J. Chem. Phys*., 1960, **33**, 676-684.

64 J. Heyd, G. E. Scuseria and M. Ernzerhof, *J. Chem. Phys.*, 2003, **118**, 8207-8215.

65 J. Heyd, G. E. Scuseria and M. Ernzerhof, *J. Chem. Phys.*, 2004, **121**,1187-1192.

66 J. Heyd, G. E. Scuseria and M. Ernzerhof, *J. Chem. Phys.*, 2006, **124**, 219906.

67 H. H. Tippins, *Phys. Rev.*, 1965, **140**, A316-A319.

68 N. Ueda, H. Hosono, R. Waseda and H. Kawazoe, *Appl. Phys. Lett.*, 1997, **71**, 933-935.

69 http://www.webelements.com.

Physical Chemistry Chemical Physics Accepted Manuscript

70 N. Todorova, T. Giannakopoulou, G. Romanos, T. Vaimakis, J. Yu and C. Trapalis, *Int. J. Photoenergy*, 2008, Article ID 534038, 9 pages.

71 A. M. Czoska, S. Livraghi, M. Chiesa, E. Giamello, S. Agnoli, G. Granozzi, E. Finazzi, C. Di Valentin and G. Pacchioni, *J. Phys. Chem. C*, 2008, **112**, 8951-8956.

72 X. Nie, S. Zhuo, G. Maeng, K. Sohlberg and Trapalis, *Int. J. Photoenergy*, 2009, Article ID 294042, 22 pages.

73 Y. Xu and M. A. A. Schoonen, *American Mineralogist*, 2000, **85**, 543-556.

Physical Chemistry Chemical Physics Accepted Manuscript

Table 1 Calculated defect formation energies in β-Ga_2O_3 under O-rich and Ga-rich conditions. The data in parentheses are obtained from a larger supercell including 80 atoms. The positions of O1, O2 and O3 in bulk are shown in Figure 1.

E_f (eV)	O-rich	Ga-rich	E_f (eV)	O-rich	Ga-rich
C-O1	2.46 (2.35)	-5.59 (-5.70)	N-O1	1.09 (1.03)	-6.97 (-7.03)
C-O2	3.99 (3.98)	-4.06 (-4.08)	N-O2	1.77 (1.78)	-6.28 (-6.27)
C-O3	3.77 (3.71)	-4.28 (-4.34)	N-O3	1.35 (1.34)	-6.70 (-6.72)
F-O1	4.20 (3.95)	-3.85 (-4.10)	Si-O1	7.24 (6.85)	-0.81 (-1.21)
F-O2	4.07 (3.82)	-3.99 (-4.23)	Si-O2	9.13 (9.11)	1.07 (1.05)
F-O3	3.84 (3.58)	-4.22 (-4.47)	Si-O3	7.41 (7.46)	-0.65 (-0.60)
P-O1	6.49 (6.38)	-1.56 (-1.68)	S-O1	5.28 (5.31)	-2.77 (-2.75)
P-O2	7.05 (7.00)	-1.01 (-1.05)	S-O2	5.31 (5.24)	-2.75 (-2.81)
P-O3	5.93 (5.86)	-2.13 (-2.20)	S-O3	4.47 (4.37)	-3.59 (-3.69)
Cl-O1	8.29 (7.94)	0.23 (-0.11)	Se-O1	7.22 (7.26)	-0.83 (-0.80)
Cl-O2	7.90 (7.59)	-0.16 (-0.46)	Se-O2	7.22 (7.16)	-0.83 (-0.90)
Cl-O3	7.39 (7.06)	-0.66 (-0.99)	Se-O3	6.25 (6.08)	-1.81 (-1.98)
Br-O1	10.09 (9.70)	2.04 (1.65)	I-O1	12.90 (12.45)	4.84 (4.40)
Br-O2	9.56 (9.22)	1.50 (1.17)	I-O2	12.26 (11.84)	4.20 (3.78)
Br-O3	8.85 (8.53)	0.80 (0.47)	I-O3	11.24 (10.81)	3.19 (2.76)

Physical Chemistry Chemical Physics Accepted Manuscript

Physical Chemistry Chemical Physics Accepted Manuscript

Figure captions

Fig. 1 (a) Bulk structure β-Ga_2O_3 with 40 atoms. The red spheres represent O atoms and the brown spheres represent Ga atoms. (b) The calculated total and project density of states for bulk β-Ga_2O_3. The Fermi level is shown by the vertical dashed line.

Fig. 2 Local structures of optimized cells for (a) C-doped, (b) Si-doped, (c) N-doped, (d) P-doped, (e) S-doped, (f) Se-doped, (g) F-doped, (h) Cl-doped, (i) Br-doped, and (j) I-doped Ga_2O_3.

Fig. 3 Total density of states (a) and projected density of states (b) for pure β-Ga_2O_3, C-doped Ga_2O_3, Si-doped Ga_2O_3, N-doped Ga_2O_3, and P-doped Ga_2O_3. The vertical dashed line represents the Fermi level.

Fig. 4 Total density of states (a) and projected density of states (b) for pure β-Ga_2O_3, S-doped Ga_2O_3, and Se-doped Ga_2O_3. The vertical dashed line represents the Fermi level.

Fig. 5 Total density of states (a) and projected density of states (b) for pure β-Ga_2O_3, S-doped Ga_2O_3, and Se-doped Ga_2O_3. The vertical dashed line represents the Fermi level.

Fig. 6 Charge density differences for the most stable structure of (a) C-doped, (b) Si-doped, (c) N-doped, (d) P-doped, (e) S-doped, (f) Se-doped, (g) F-doped, (h) Cl-doped, (i) Br-doped, and (j) I-doped Ga_2O_3. The yellow and cyan volumes represent zones of electron depletion and accumulation, respectively.

Fig. 7 Schematic representation of the calculated VBM and CBM positions of X-doped Ga_2O_3 with reference to those of pure Ga_2O_3.

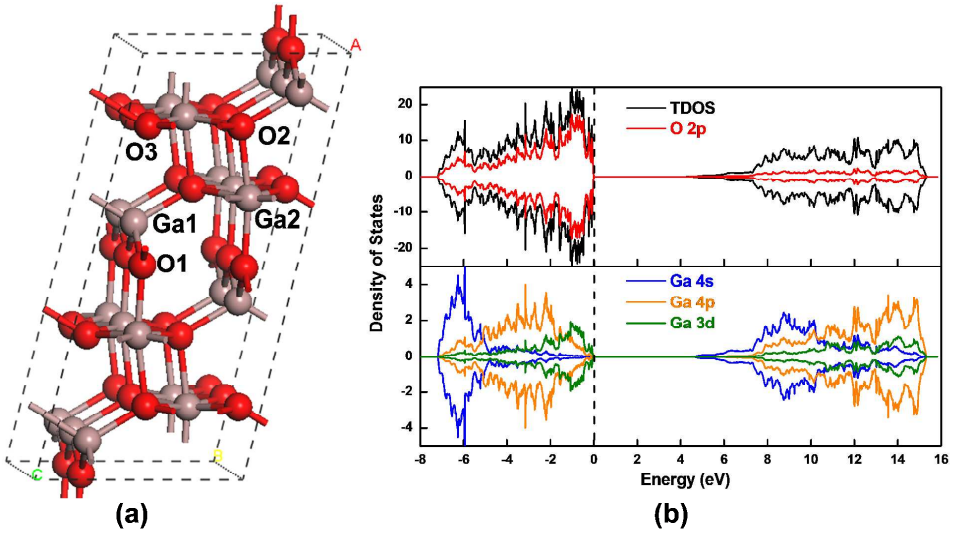

Fig. 1

Physical Chemistry Chemical Physics Accepted Manuscript

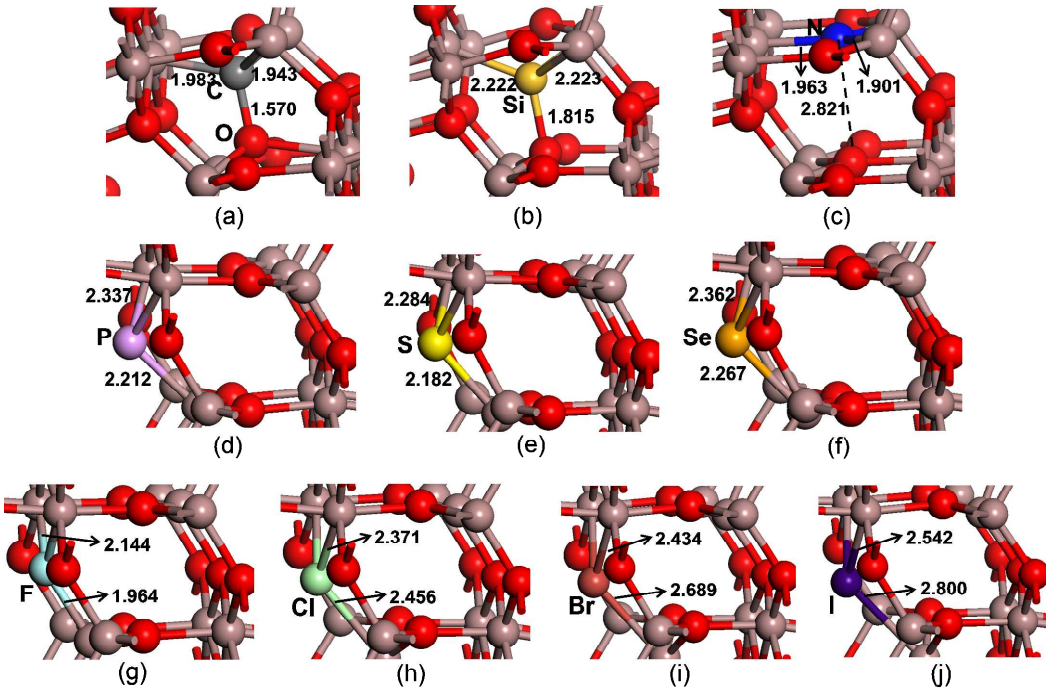

Fig. 2

Physical Chemistry Chemical Physics Accepted Manuscript

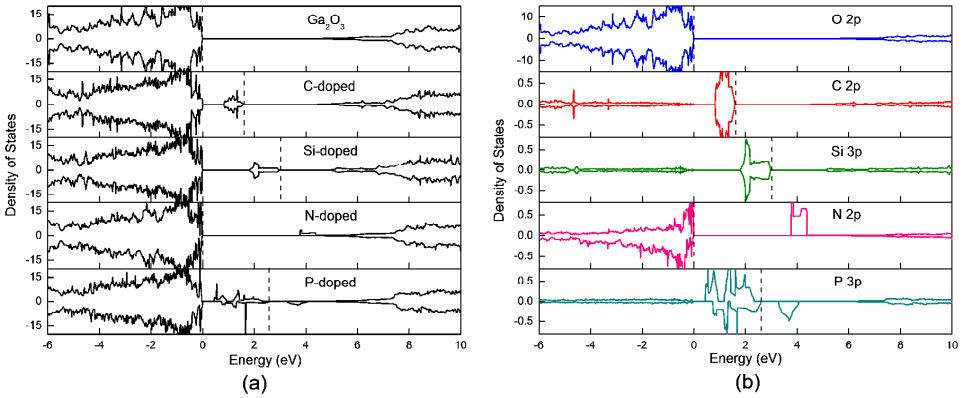

Fig. 3

Physical Chemistry Chemical Physics Accepted Manuscript

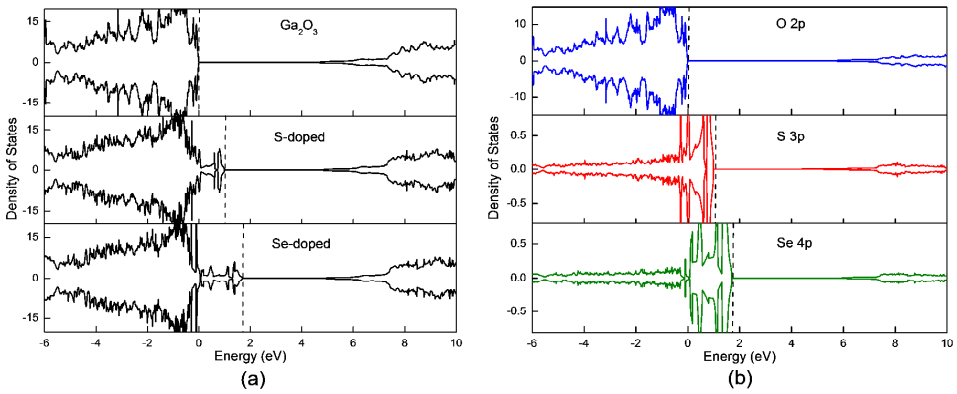

Fig. 4

Physical Chemistry Chemical Physics Accepted Manuscript

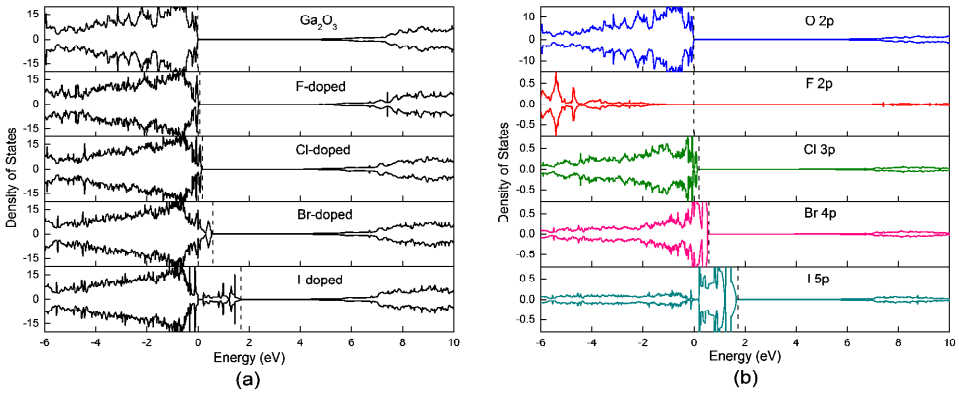

Fig. 5

Physical Chemistry Chemical Physics Accepted Manuscript

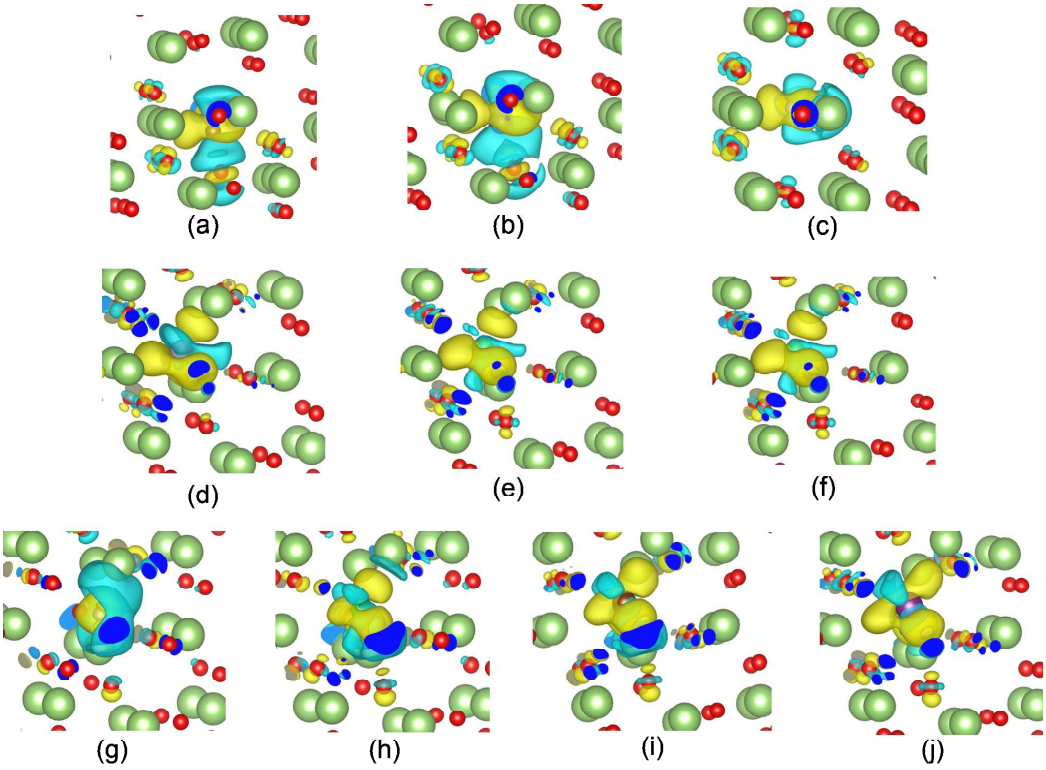

Fig. 6

Physical Chemistry Chemical Physics Accepted Manuscript

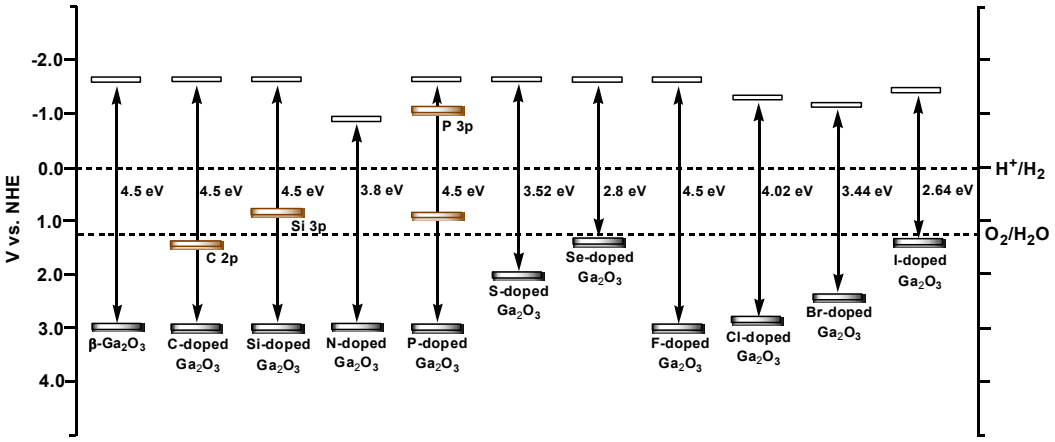

Fig. 7

Physical Chemistry Chemical Physics Accepted Manuscript